Radius Determination of Exoplanets and the Typicality of Earth

Haley Bates-Tarasewicz

Abstract

Understanding exoplanets is key to understanding the typicality of our own solar system. The creation and evolution of Earth cannot be understood without first understanding how other planets are created and evolve. Knowing how common earth-like planets are is a start to understanding how representative our own system is as a whole. Exoplanet radii were determined using the transiting exoplanet method to allow comparison of physical traits between extrasolar planets and the planets orbiting our sun. All exoplanets imaged were of comparable size to Jupiter. However, due to the limitations of the transit method, better exoplanet imaging techniques have to be furthered before these findings can be understood in context.

Introduction

Exoplanets are planets that orbit star systems other than our own. Exoplanets can be detected in a variety of ways, one of which is via photometric transits. Transits occur when a star system is aligned with Earth such that a planet orbiting will appear to pass in front of, or transit, the host star. In this way, the planet blocks some of the light from the host star, causing a distinctive dip in the light curve[1]. The planets that can be detected with this method are occasionally quite different from Earth[2], which makes our own star system seem atypical by comparison[3].

Studying exoplanets can help further understanding of the underlying mechanisms of planet formation. To understand how planets form, it's useful to know how similar planets in other star systems are to our own Earth. By analyzing the light curve produced when an exoplanet transits its host star (Figure. 1) the radius of the planet can be deduced[4].

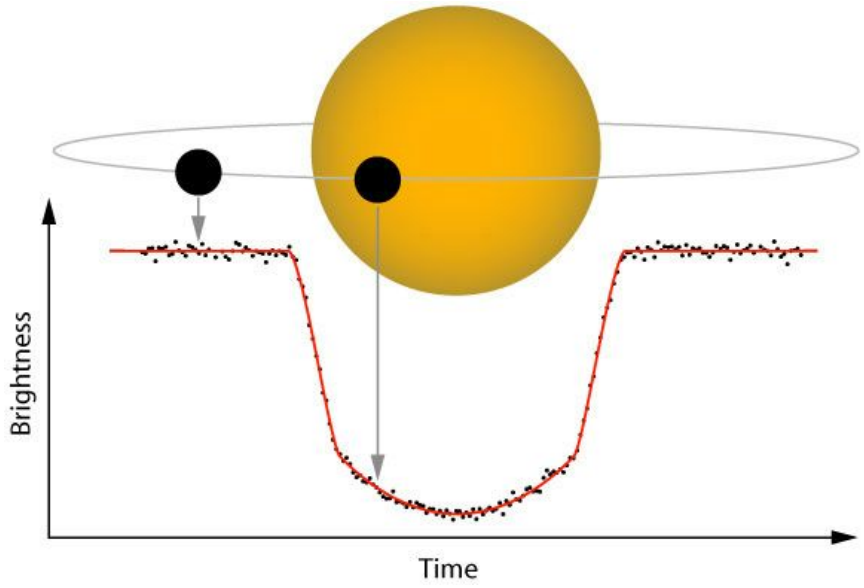

Figure 1: The transit method of detecting and imaging exoplanets[1]

1: Introduction to Differential Photometry. (2013, February 18). Retrieved November 1, 2015.

---

1 Schneider, J.; Dedieu, C.; Le Sidaner, P.; Savalle, R.; Zolotukhin, I., 2011. Defining and cataloging exoplanets: the exoplanet.eu database. Astronomy & Astrophysics, Volume 532, id.A79, 11 pp.

2 Marcy, G.; Butler, R. P.; Fischer, D.; Vogt, S.; Wright, J. T.; Tinney, C. G.; Jones, H. R. A., 2005. Observed Properties of Exoplanets: Masses, Orbits, and Metallicities. Progress of Theoretical Physics Supplement, No. 158, pp. 24-42.

3 Udry, Stéphane; Santos, Nuno C., 2007. Statistical Properties of Exoplanets. Annual Review of Astronomy & Astrophysics, vol. 45, Issue 1, pp.397-439.

4 Weiss, Lauren M.; Marcy, Geoffrey W., 2014. The Mass-Radius Relation for 65 Exoplanets Smaller than 4 Earth Radii. The Astrophysical Journal Letters, Volume 783, Issue 1, article id. L6, 7 pp. (2014).

Determining any physical properties of exoplanet can be used to learn more about the star system as a whole[5]. Knowing more about the properties of planets outside our solar system can help to better understand the planets within it.

Several exoplanets were observed during the months of September and October (2015) to try to better understand the planets that form in other star systems as well as our own.

Targets

All transit candidates were observed between September and October 2015 at MIT's Wallace Astrophysical Observatory. Candidates were chosen such that they would be visible at Wallace Astrophysical Observatory given the limitations of the site.

All candidates were chosen such that the magnitude of the host star was well within the lower limit detectable with the equipment at Wallace (~18th magnitude)[6]. Transit candidates were also chosen such that the depth of transit is visible with the resolution of the available instrumentation (~ 10 milimags)[7]. Transit candidates were optimized such that the entirety of the transit would be viewable in one night, considering both elevation and duration. To be visible at Wallace Observatory, a target must be above 20° in elevation, and due to travelling restrictions, the full transit must be less than 3h total[8]. Full observational circumstances for each target are located in Table 1 below.

5 Seager, S.; Kuchner, M.; Hier-Majumder, C. A.; Militzer, B., 2007. Mass-Radius Relationships for Solid Exoplanets. The Astrophysical Journal, Volume 669, Issue 2, pp. 1279-1297.

6 Brothers, T.

7 Brothers, T.

8 Brothers, T.

Table 1: Observational Circumstances for Observed Exoplanet Transits at Wallace Astrophysical Observatory in September and October [1]

Date (EDT)	Transit	Apparent Magnitude (R)	Delta Magnitude (milimags)	Elevation (start, mid, end)	Time (EDT) (start, mid, end)	Right Ascension (J2000)	Declination (J2000)
9/14/2015	Tres-3 b	12.1	29.3	37°, 30°, 24°	22:44—23:24—00:04	17 52 07.02	+37 32 46.2
10/5/2015	Tres-1 b	11.2	19.8	53°, 39°, 26°	22:01—23:16—00:31	19 04 09.84	+36 37 57.5
10/16/2015	Kepler-6 b	15.6	10.4	72°, 52°, 34°	20:25—22:23—00:21	19 47 20.94	+48 14 23.8
10/25/2015	Kepler-45 b	15.7	34.2	77°, 71°, 65°	20:53—21:25—21:57	19 31 29.50	+41 03 51.3

1: Introduction to Differential Photometry. (2013, February 18). Retrieved November 1, 2015.

All data were to be analyzed via on chip standard stars. Standard stars were chosen such that they were easily in the target star field during observation, and care was taken to ensure they were within 1.5 magnitudes of the target star.

Effort was made to pick comparison stars brighter than the target, so the signal to noise ratio would be limited by the target star rather than the comparison star. In many cases, however, choosing slightly dimmer stars was unavoidable simply due to the stars available on chip.

Three comparison stars for each transit were considered. Table 2 below shows the specifications for each comparison star according to the transit candidate. Complete finder charts for each transit candidate are located in the appendix.

Table 2: Comparison Star Specification for Transit Star Fields (see appendix for finding charts)[1,2]

Transit	Right Ascension (J2000)	Declination (J2000)	Magnitude (R)
Tres-3 b	17 52 18.57	+37 35 56.22	13.4
	17 52 5.36	+37 30 42.48	13.9
	17 51 42.88	+37 31 13.12	13.0
Tres-1 b	19 04 09.35	+36 39 20.09	12.8
	19 04 07.91	+36 40 11.97	11.2
	19 03 39.34	+36 37 25.94	10.7
Kepler-6 b	19 47 08.6	+48 15 28.58	14.4
	19 47 00.23	+48 17 06.73	12.6
	19 46 55.64	+48 12 25.92	14.0
Kepler-45 b	19 31 31.91	+41 04 54.22	15.1
	19 31 20.60	+41 02 12.04	15.4
	19 31 29.46	+41 01 13.21	14.9

1: This research has made use of the VizieR catalogue access tool, CDS, Strasbourg, France. The original description of the VizieR service was published in A&AS 143, 23

2: The USNO-A2.0 Catalogue. (1998). Retrieved November 1, 2015.

Methods of Observation

All data was taken at Wallace Astrophysical Observatory. Two telescopes were used to collect data. The Ealing 16” telescope, and pier 3 14” Celestron telescope.

The 16” telescope was originally going to be used for all collected data, however, due to unfavorable weather conditions and telescope need, the 14” telescope was used as well.

The 16” telescope is the largest available telescope for student use at Wallace Observatory, and has the lowest detectable magnitude limit of all available telescopes. Advantage of this fact was going to be taken to try to get the signal to noise ratio of the dimmer transit candidates as favorable as possible. However as it turned out, the two dimmest candidates were unavoidably observed with the 14” telescope.

Both telescopes used in data collection made use of an SBIG STL-1001E CCD Camera. Full specifications for both telescopes and the camera are located in Tables 3, 4, and 5 below.

Table 3: Specifications for Ealing 16" Telescope[1]

Diameter (inches)	16
Focal Length (mm)	4429.8
Primary Instrument	SBIG STL-1001e
Field of View (arcminutes)	19.07 x 19.07
Plate Scale (arcseconds/pixel)	1.11
Filters	Clear, B, V, R, I, VR

1: Brothers, T. (2015, June 18). Retrieved November 1, 2015.

Table 4: Specifications for 14" Celestron C14 Schmidt-Cassegrain Telescope[1]

Diameter (inches)	14
Focal Length (mm)	3910
Primary Instrument	SBIG STL-1001e
Field of View (arcminutes)	20.65 x 20.65
Plate Scale (arcseconds/pixel)	1.21
Filters	Clear, B, V, R, I, VR

1: Brothers, T. (2015, June 18). Retrieved November 1, 2015.

Table 5: Instrumental Specifications for SBIG STL-1001E CCD Camera[1]

Min / Max Exposure Times (sec)	0.01 / 3600
Max Counts Unbinned	~64000
Gain (electrons)	2.0
Pixel array	1024 x 1024 active element
Pixel dimensions (square microns)	24
Working Temperature Range (deg C)	-15 to -25

1: Brothers, T. (2015, June 18). Retrieved November 1, 2015.

Data

Four nights of data total were taken over the months of September and October 2015. Each night, the the telescopes were set up in accordance with Wallace Observatory's instructions and guidelines and focused. The telescopes were then slewed to the correct right ascension and declination of the target transit candidate, star hopping to the correct target.

Each night before any data was taken, 10 0s exposure bias frames were taken as a diagnostic tool as well as for use in later data reduction.

Exposure times for science frames were determined by a combination of TA input and adjustment so the counts from the target star fell on the middling/linear range of the CCD. The R filter was used for all data as all transit candidates and comparison stars were brightest in the R band. After the exposure time and filter was set, data was taken until time constraints dictated we leave Wallace (usually 3.5hours).

After science frames were taken, 10 closed-shutter dark frames with exposure times matching that of the science frames were taken for later calibration.

A full breakdown of all data and calibration images taken in September and October is located in Table 6 below.

Table 6: Data Taken at Wallace Astrophysical Observatory in September and October 2015

Transit	Date (2015) (EDT)	Frame	Exposure Time (seconds)	Filter	Data Amount (Images)	Weather	Telescope
Tres-3 b	Sep. 14	Bias	0	n/a	10	Clear	Ealing 16in
		Dark	20	n/a	10		
		Light	20	R	382		
Tres-1 b	Oct. 5	Bias	0	n/a	10	Clear	Ealing 16in
		Dark	30	n/a	10		
		Light	30	R	354		
Kepler-6 b	Oct. 16	Bias	0	n/a	10	Clear	14in Celestron
		Dark	20	n/a	10		
		Light	20	R	716		
Kepler-45 b	Oct. 25	Bias	0	n/a	10	Cloudy	14in Celestron
		Dark	75	n/a	10		
		Light	75	R	173		

Data Reduction and Preliminary Analysis

All reduction of data was done in AstroImageJ. AstroImageJ makes use of dark/bias subtraction and flat division.

All calibration frames (bias, dark, flat) are averaged together to create master bias/dark/flat frames. Bias and dark frames were taken each night of data collection, however because of time constraints, sky flats were not able to be collected, so dark-subtracted library flats were used instead.

First the master bias is subtracted from all frames to remove the counts produced by the camera reading out an image. Then the master dark is subtracted from the science frames to remove the counts produced by the camera during an exposure. Then, the science images are divided by the reduced flats to remove any imperfections with the telescope or imaging equipment. Figure 2 below illustrates this process.

Figure 2: Calibration images and reduction process using dark/bias subtraction and flat division.

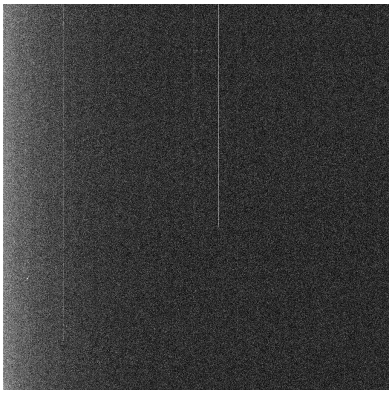

Bias

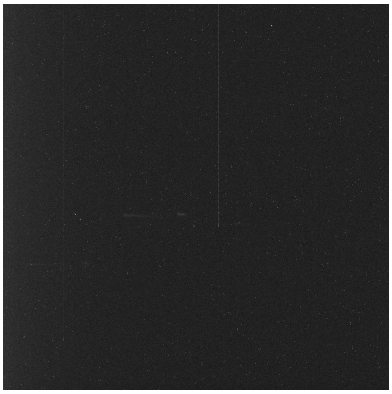

Dark

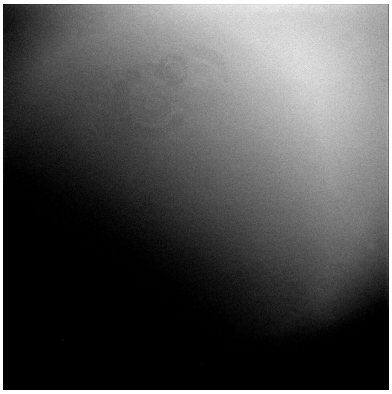

Flat

Raw Data

Reduced Image

After images were reduced, they were analyzed using multi-aperture photometry in AstroImageJ. AstroImageJ uses circular apertures with a concentric background annulus positioned such that little to no target starlight bleeds into it. Aperture and annulus sizes were determined by plotting the seeing profile of the target star and adjusting AstroImageJ's recommended values such that the source aperture contained all relevant source signal, and the background contained no source from stars. An example of this can be seen in Figure 3 below. Other seeing profiles and apertures/annuli for other nights can be seen in the Appendix.

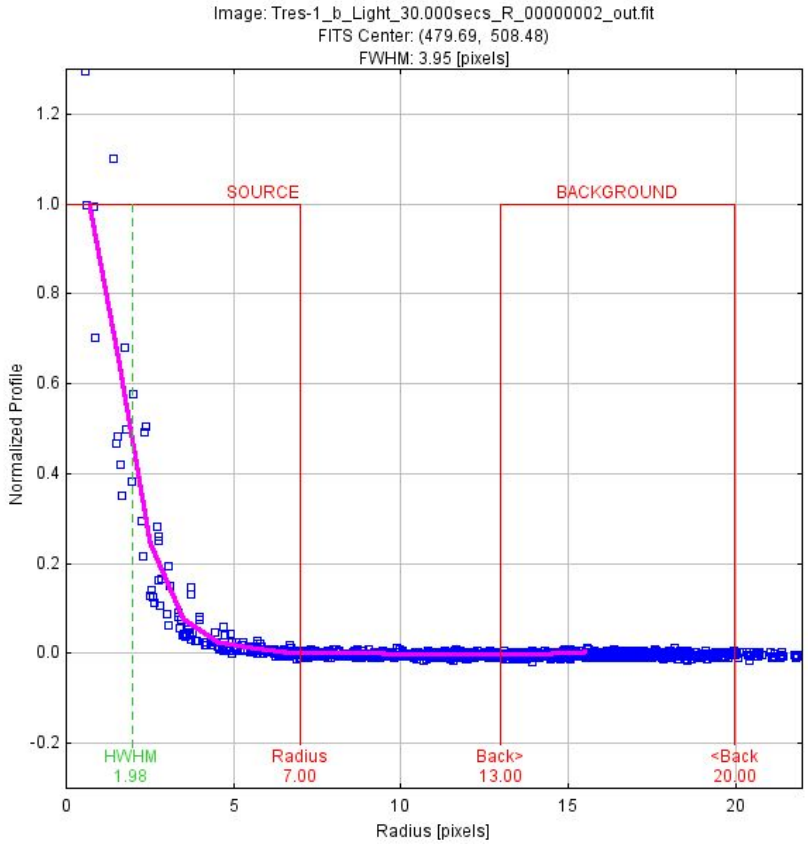

Figure 3: Seeing profile and aperture/annulus radii for Tres-1 b (see other seeing profiles etc. in Appendix)

To ensure that the comparison stars weren't influencing the data, all comparison stars were tested for quality before analysis began. Stars were checked for uniformity by plotting Relative Flux vs Time and ensuring the flux stayed constant over the course of the night. All comparison stars were verified in this way. An example of one of these comparison star tests can be seen in Figure 4 below. For comparison star verifications of other nights of data, see the Appendix.

Figure 4: Comparison star quality test for Tres-1 b to determine flux uniformity (see other comparison star quality tests in Appendix)

Once all comparison stars were verified as constant over the course of the night, they were used to analyze the target transit candidate. Multi-aperture photometry was again done in AstroImageJ. The relative flux of the transit candidate to the average of the target stars was recorded. Figure 5 below shows the aperture and target locations for one night. Other nights can be seen in the Appendix.

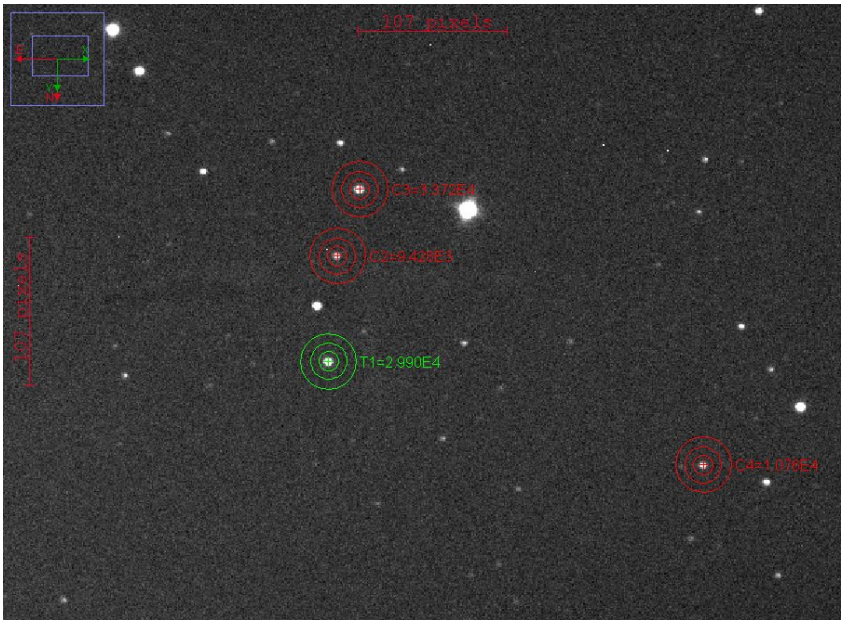

Figure 5: Comparison stars and multi-aperture photometry processing for Tres-1 b (see other aperture placement and comparison stars in Appendix)

Table 7 details the aperture and annulus radii for all datasets, as calculated by the method discussed in Figure 3 above.

Table 7: Apertures and background annuli for multi-aperture photometry data analysis of exoplanet transit data

Transit	Radius of Object Aperture (px)	Inner Radius of Background Annulus (px)	Outer Radius of Background Annulus (px)
Tres-3 b	6	11	17
Tres-1 b	7	13	20
Kepler-6 b	6	11	17
Kepler-45 b	5	9	14

Once the relative flux of the target transit candidate to the comparison stars was calculated, it was plotted and analyzed in MATLAB. All four nights were plotted in this manner. Out of all four nights, only the plot below (Figure 6) of data taken of Tres-1 b on 10/05/2015 showed a transit dip.

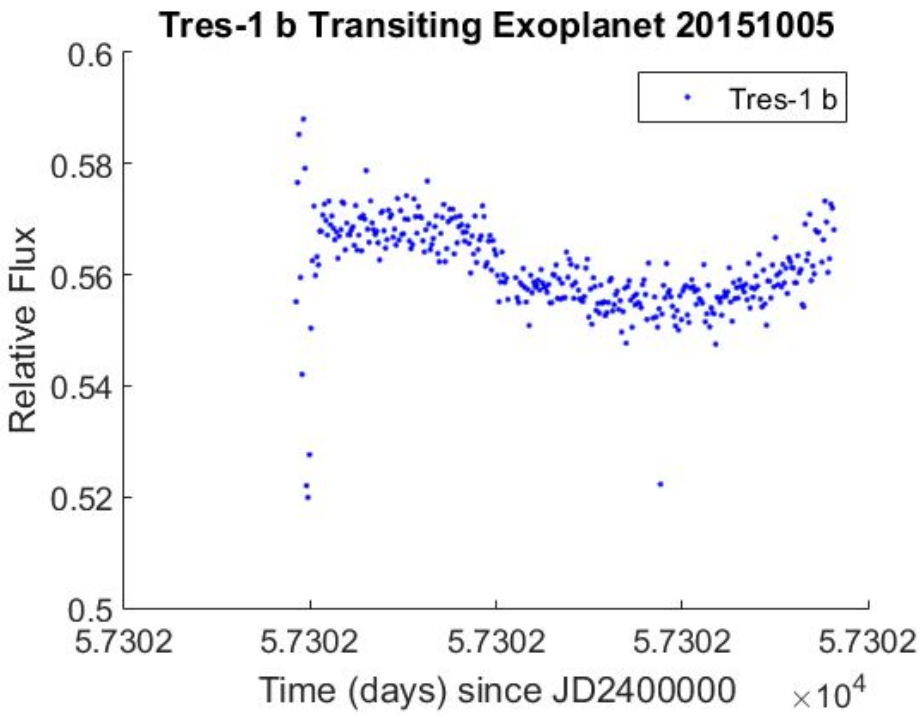

Figure 7: Relative Flux vs Time of transiting exoplanet Tres-3 b on October 5th 2015 (see other relative flux plots in Appendix)

Figure 8 shows the relative flux vs time of the data taken of Tres-3 b on 9/14/2015. There was unfamiliarity with the software used to plan transit observations, and due to an unfortunate mistake, the observation took place on the wrong night. For this data, no transit dip was expected. The sudden spike and break in the data is due to cloud interference.

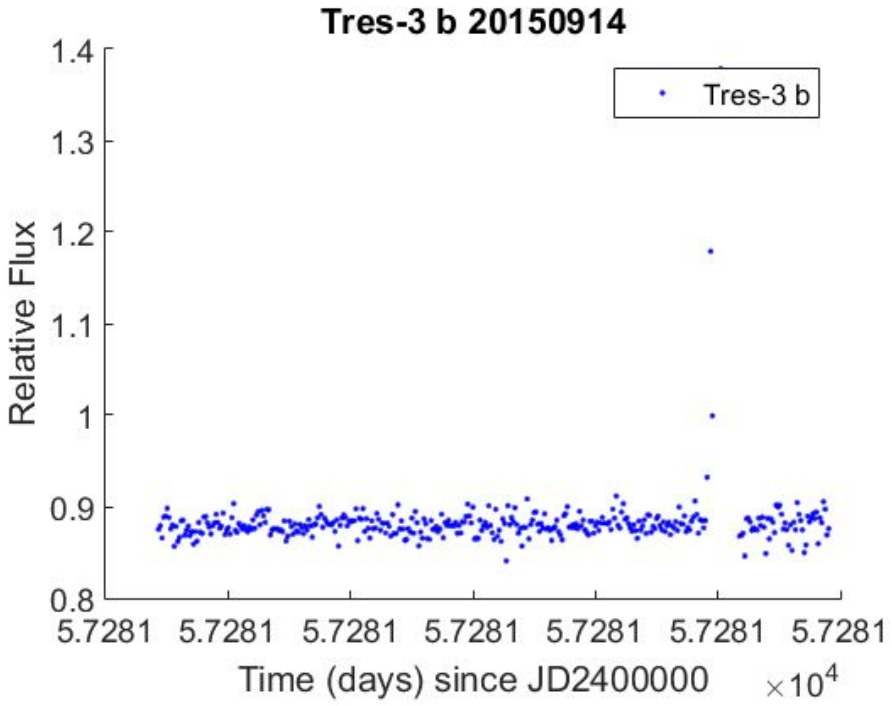

Figure 8: Relative Flux vs Time of transiting exoplanet Tres-3 b on September 14th 2015

Figure 9 below shows a similar plot of relative flux vs time of data taken of Kepler-6 b on 10/16/2015. This plot doesn't show a dip, however, the predicted depth of transit was only 10.4 milimags, which is right at the very lower limit of the capabilities of Wallace Observatory. It is not surprising that a transit dip wasn't observed. Problems with dew and clouds caused some scattering in the beginning and middle of the plot.

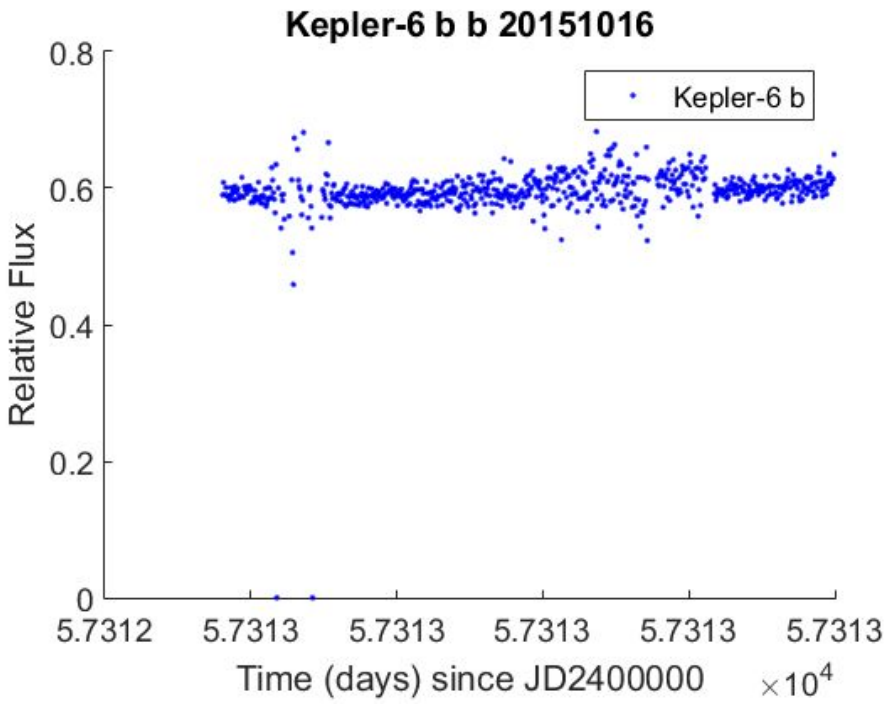

Figure 9: Relative Flux vs Time of transiting exoplanet Tres-3 b on October 16th 2015

Figure 10 shows the relative flux of Kepler-45 b, taken on 10/25/2015. The night ended up being much cloudier than expected, so most of the data was taken under nearly full cloud cover. After rejecting frames where no stars were visible and only analyzing ones where the target was resolved at all, there wasn't enough data to say that a transit did or didn't occur. No transit dip was expected for this data.

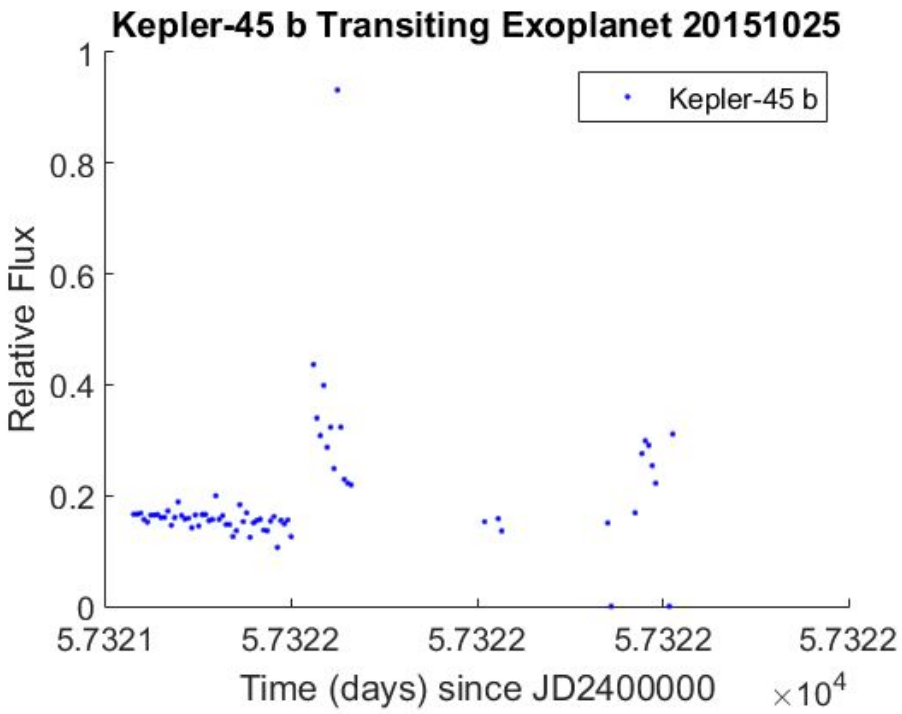

Figure #: Relative Flux vs Time of transiting exoplanet Kepler-45 b b on October 25th 2015

Because of the challenges with software that resulted in the 9/14/2015 data being unusable, and because of poor weather conditions on 10/25/2015, only the data taken on 10/05/2015 and 10/16/2015 will be considered for further analysis.

Results and Analysis

While using the transit method, planetary/stellar radii are related to the transit dip by $\Delta f = \left(\frac{r}{R}\right)^2$ where f is the flux, r is the radius of the exoplanet, and R is the stellar radius.[9]

Table 8 shows the published stellar radii in terms of the sun's radius for each analyzable night.

9 Schneider, J.; Dedieu, C.; Le Sidaner, P.; Savalle, R.; Zolotukhin, I., 2011. Defining and cataloging exoplanets: the exoplanet.eu database. Astronomy & Astrophysics, Volume 532, id.A79, 11 pp.

Table 8: Transiting exoplanet host star physical properties[1, 2]

Transit	Published Stellar Radius (M_{Sun})
Kepler-6 b	1.39 0.02
Tres-1 b	0.87 0.02

1: This research has made use of the Exoplanet Orbit Database and the Exoplanet Data Explorer at exoplanets.org.
2: Han, E., Wang, S., Wright, J., Feng, K., Zhao, M., Fakhouri, O., . . . Hancock, C. (2014). Exoplanet Orbit Database. II. Updates to Exoplanets.org. *126*(943), 827-837. Retrieved November 1, 2015, from http://adsabs.harvard.edu

Analysis for the transit recorded on 10/05/2015 of Tres-1 b began by calculating the weighted mean of both the baseline non-transiting star flux and the base of the transit dip were calculated in MATLAB using the uncertainty reported by AstroImageJ during preliminary analysis. Then, the standard deviation for both the baseline and the transit was determined using MATLAB.

Using these values, the transit depth for the data taken of Tres-1 b on 10/05/2015 after propagating error was determined to be 0.018 ± 0.013, which is a dimensionless number that represents the ratio of the planetary radius to the stellar radius squared.

Using $\Delta f = \left(\frac{r}{R}\right)^2$ and the published stellar radius of the host star of Tres-1 b, the radius of the planet was determined to be 1.235 $R_{Jupiter}$ ± 0.35, in terms of Jupiter's radius.

For the case of the data taken on 10/16/2015 of Kepler-6 b, no transit dip was recorded, so instead of determining what the transit dip was, the largest possible transit dip given the data was calculated. Analysis began by calculating the weighted mean of the entire dataset at 0.596 using MATLAB. From this, the standard deviation of the entire set was calculated to be 0.039, also using MATLAB.

The largest transit depth that could have taken place is 0.039, which represents the ratio of the planetary radius to the stellar radius squared.

Again using $\Delta f = \left(\frac{r}{R}\right)^2$ and the published stellar radius of the host star of Kepler-6 b, the radius of the planet was determined to be a maximum of 0.87 $R_{Jupiter}$, in terms of Jupiter's radius.

No data points were rejected for either night of data.

Table 9 shows all of the values calculated in the analysis of both nights of data.

Table 9: Calculated values for the determination of exoplanet radii

Transit	Weighted Mean (baseline, transit dip)	Standard Deviation (baseline, transit dip)	Transit Depth	Calculated Radius ($R_{Jupiter}$)
Tres-1 b	0.455, 0.463	0.033, 0.478	0.018 ± 0.013	1.235± 0.35
Kepler-6 b	0.596, n/a	0.039, n/a	0.039 (upper bound)	0.87 (upper bound)

Conclusions

The research done in September and October 2015 at Wallace Astrophysical Observatory on transiting exoplanets leads to several different tentative conclusions to the question of the typicality of our own star system.

It could be that our solar system is very atypical in that it contains very small planets far away from the host star. The two exoplanets analyzed by this research both have radii comparable to that of Jupiter, and orbit very quickly around their host star. This could be indicative of a galaxy full of very large planets, where small ones are rare or less common.

Far more likely, the limitations of the transit method lead to the detection of only very large planets. Due to the restrictions of the transit method, not all exoplanets can be detected in this manner. In many cases, the planet is too small to block a detectable amount of its host star's light, or orbits too slowly for it to be detected. To better understand our own star system, more reliable methods of exoplanet detection will need to be developed.

Appendix

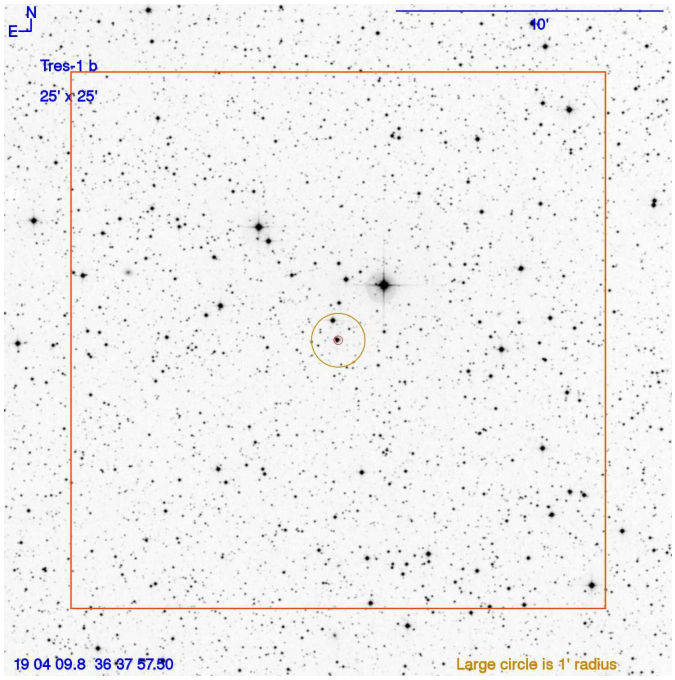

Appendix 1: Tres-1 b finding chart. Target circled in center.

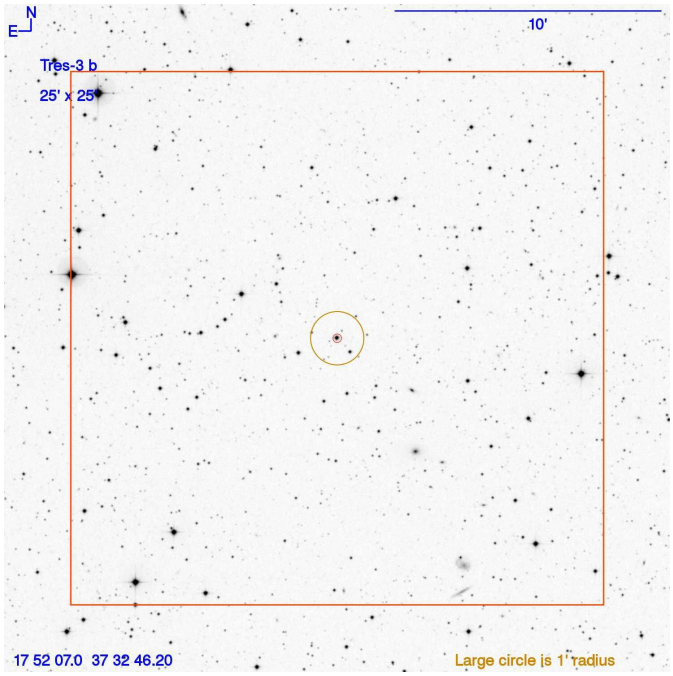

Appendix 2: Tres-3 b finding chart. Target circled in center.

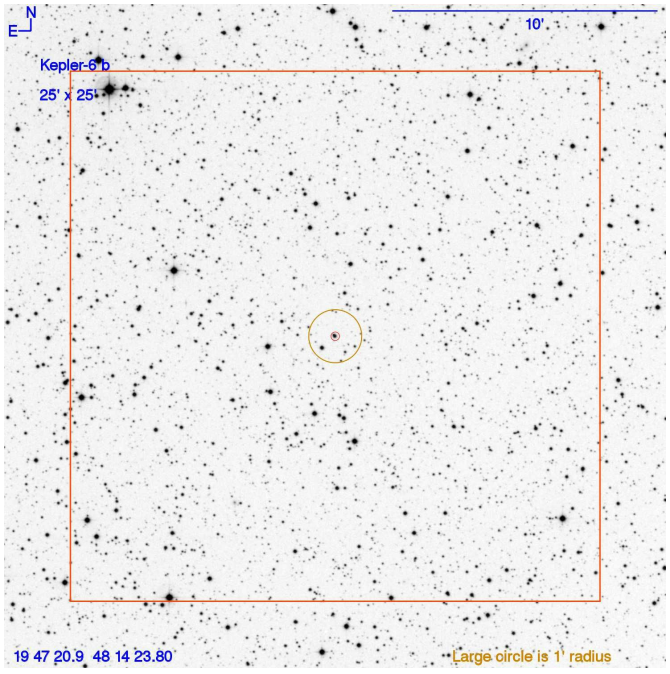

Appendix 3: Kepler-6 b finding chart. Target circled in center.

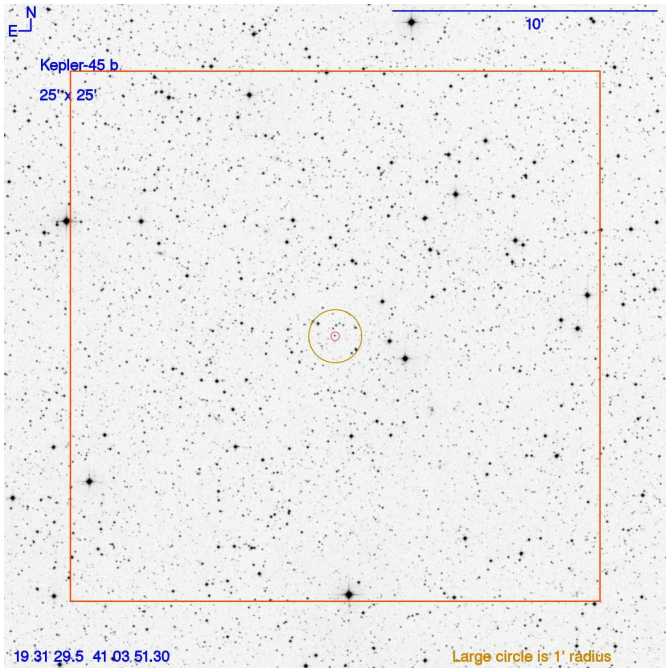

Appendix 4: Kepler-45 b finding chart. Target circled in center.

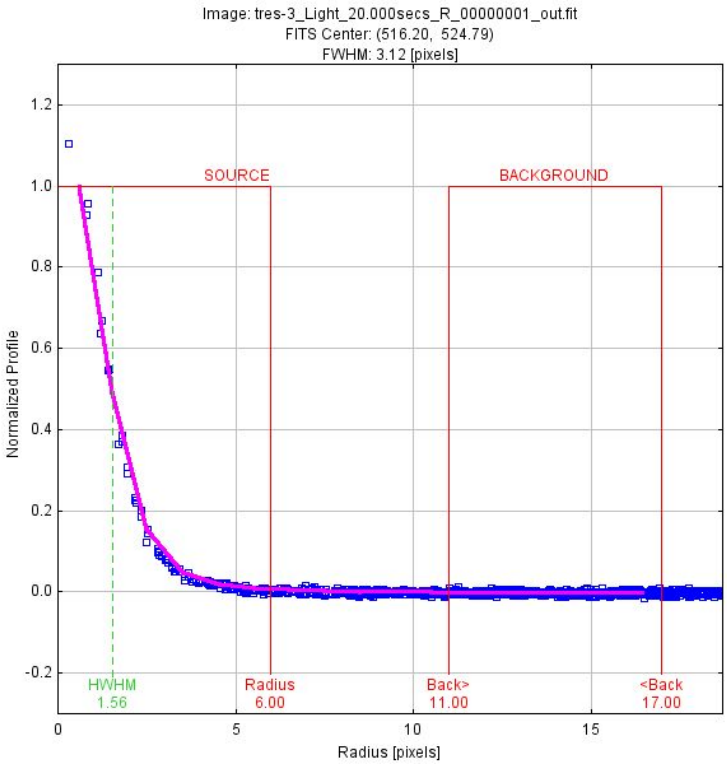

Appendix 5: Seeing profile and aperture/annulus radii for Tres-3 b

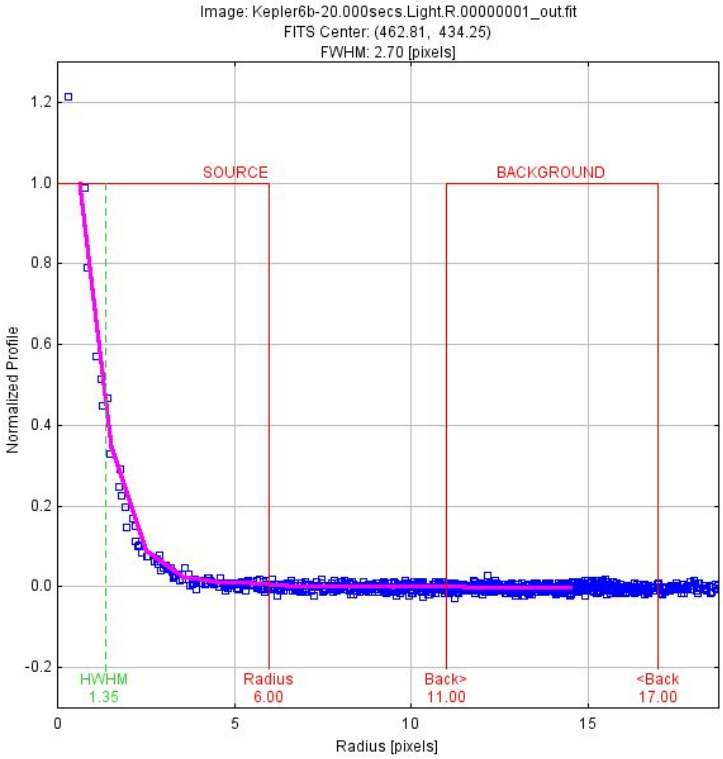

Figure 6: Seeing profile and aperture/annulus radii for Kepler-6 b

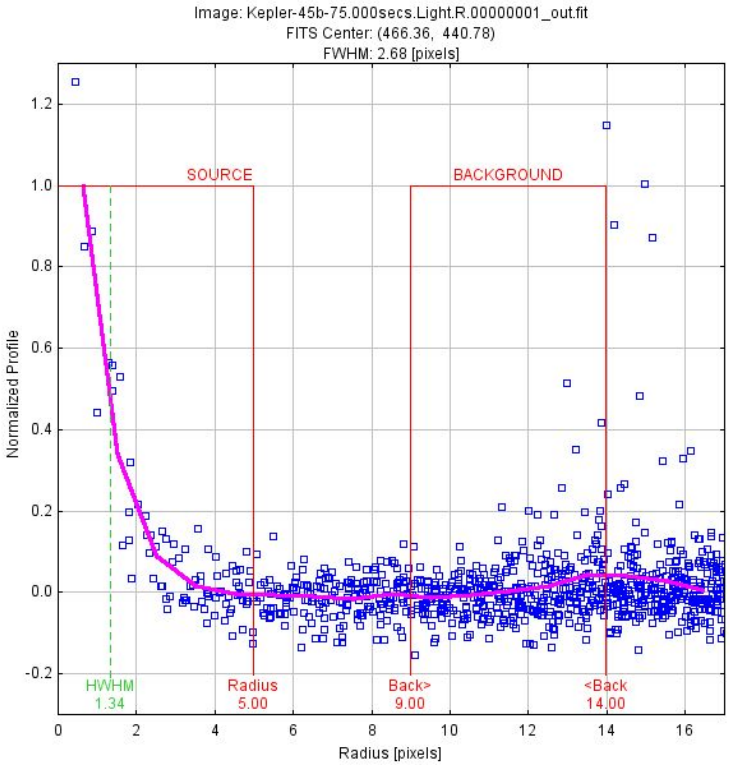

Appendix 7: Seeing profile and aperture/annulus radii for Kepler-45 b

Appendix 8: Comparison star quality test for Tres-3 b to determine flux uniformity

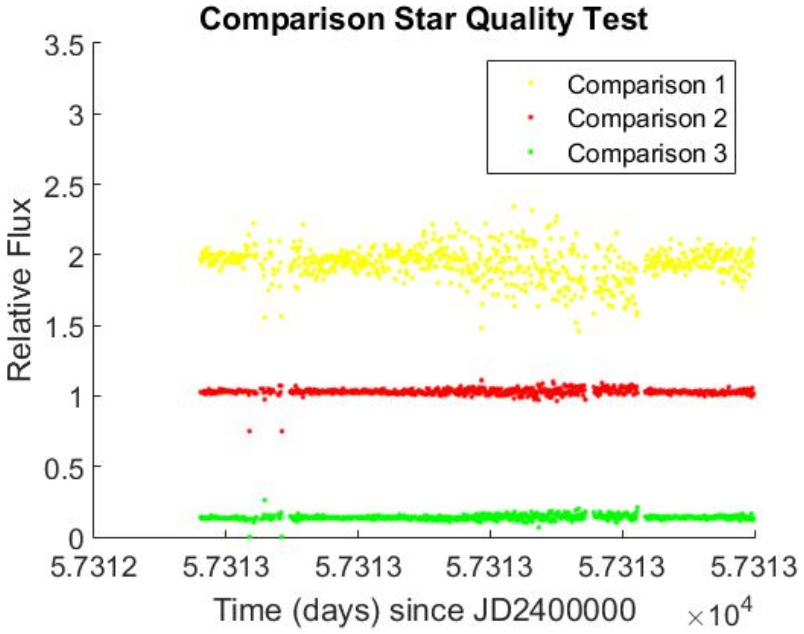

Appendix 9: Comparison star quality test for Kepler-6 b to determine flux uniformity

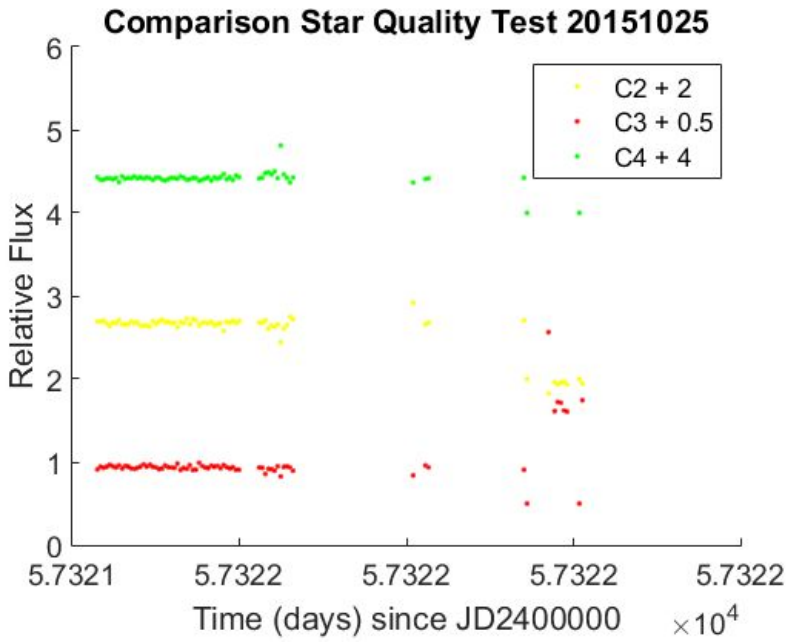

Appendix 10: Comparison star quality test for Kepler-45 b to determine flux uniformity

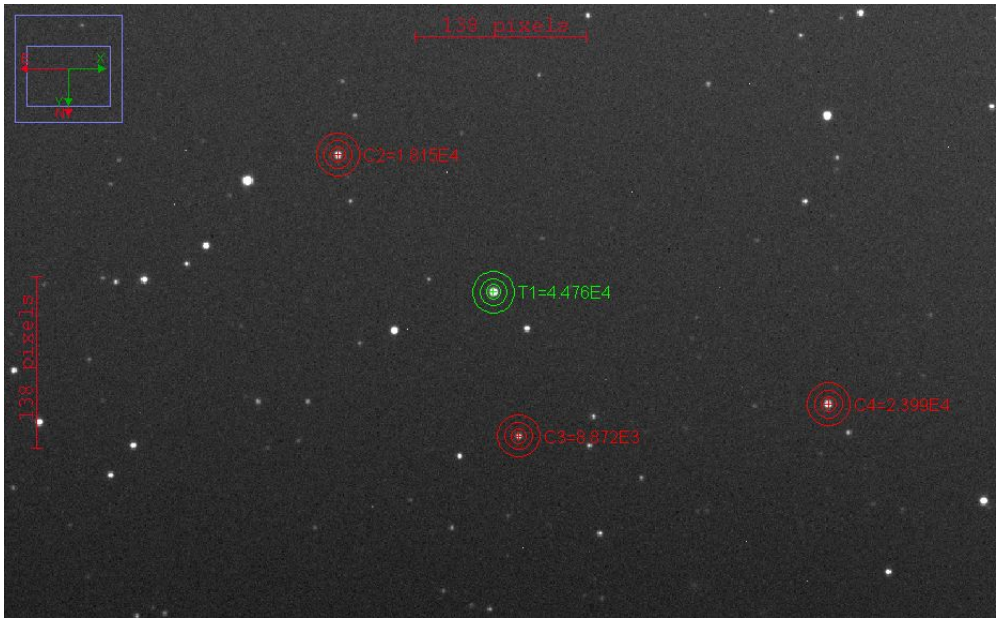

Appendix 11: Comparison stars and multi-aperture photometry processing for Tres-3 b

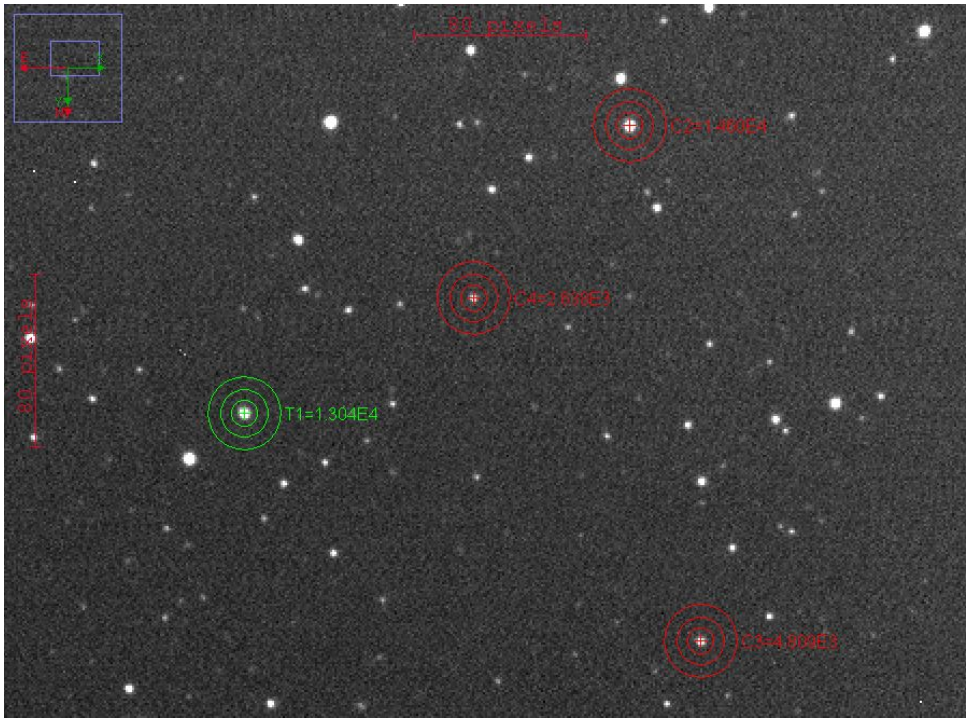

Appendix 12: Comparison stars and multi-aperture photometry processing for Kepler-6 b

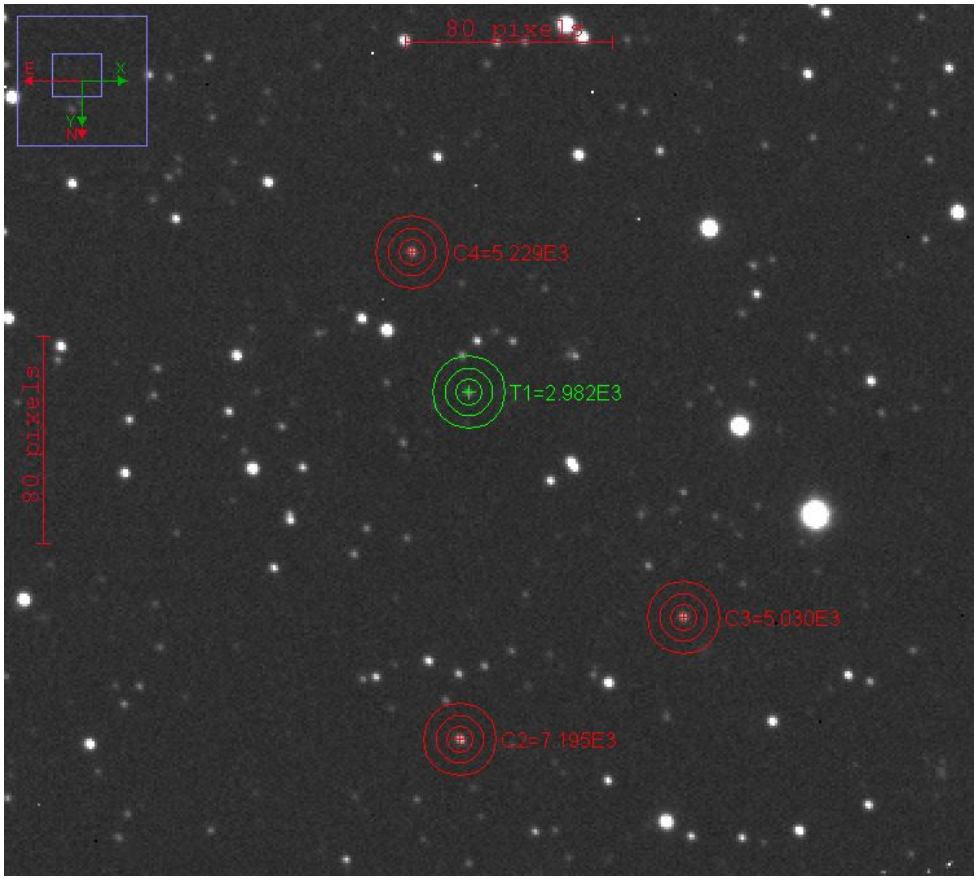

Appendix 13: Comparison stars and multi-aperture photometry processing for Kepler-45 b